Nuclear Reactions of Tantalum with 5.7-Gev Protons*

J. ROBB GROVER
Chemistry Department, Brookhaven National Laboratory, Upton, New York and Lawrence Radiation Laboratory, University of California, Berkeley, California

(Received January 15, 1962)

Radiochemically determined cross sections are reported for sixty-seven of the nuclides which appear as products of the nuclear reactions between 5.7-Gev protons and tantalum, and upper or lower limits are reported for thirty additional product nuclides. These data are distributed throughout the range of mass numbers $7<A<180$. The mass yield distribution obtained from the data is similar to the distribution reported by Wolfgang *et al.* for the interactions of 3-Gev protons with lead, and is consistent with their observations that (1) all mass numbers less than that of the target are represented with cross sections of at least a few millibarns; and (2) there is no obvious fission peak, even though a fission peak is clearly seen at lower bombarding energies (0.3 to 0.5 Gev). However, an objective criterion is devised which, when applied to the data, gives a result supporting the view that at least one reaction process other than spallation (presumably fission) is necessary to explain the observed shape of the mass yield distribution. Although for product mass numbers above $A\approx70$ most of the measured cross sections represent "chain yields" of neutron-deficient nuclides, it is possible to determine the approximate locus in the N,Z plane of the line of isobaric independent yield maxima, up to $A\approx150$. This line is compared with various calculated lines, given in the high-energy nuclear evaporation paper by Dostrovsky, Rabinowitz, and Bivins, in an effort to extract new information on the average excitation energy and neutron deficiency (or excess) of the nuclear evaporation progenitors as functions of the mass number, and on the nuclear state density parameter a.

INTRODUCTION

EXPERIMENTAL investigations of the reactions of nuclei with high-energy (>0.1-Gev) nucleons should provide data useful for the study of certain aspects of nuclear structure, because the De Broglie wavelength of the incident nucleons is small compared to nuclear dimensions. Unfortunately, the interpretation of the data is difficult because the experimental probe is so disruptive to the target nucleus that the features of the data which depend on nuclear structure are badly scrambled with the effects of the very complicated and imperfectly known reaction mechanisms. Also, for incident nucleons with energies greater than about 1 Gev it is still not certain that all of the important reaction mechanisms have been identified. The knowledge of nuclear structure and high-energy nuclear reaction mechanisms that has been achieved through radiochemical investigations is described in several recent review papers.[1–3] One of the papers[1] includes a bibliography of radiochemical cross-section measurements reported up to February, 1959.

To provide a basis for the interpretation of experimental data, many workers have performed calculations to explore the characteristics of the intranuclear cascade process,[4] and of the de-excitation of highly excited nuclei via particle evaporation.[5] Based on such calculations, analyses have been made of some of the high-energy nuclear reaction data, such as mass yield distributions, energy spectra, and angular distributions of the "gray prongs" measured in emulsion studies, etc., and have met with noteworthy success for incident nucleons with energies in the range 0.1 to 0.5 Gev[4,6]; to a somewhat lesser degree they have also been successful for incident energies from 0.5 to 1.8 Gev.[4] It therefore seems reasonable to try to use some of the results of these calculations qualitatively, to help assess the information content and usefulness of the data reported in this paper, even though, strictly speaking, some of the calculations are not properly applicable for incident nucleons of 5.7 Gev.

EXPERIMENTAL DETAILS

Targets. For most of the measurements, the target consisted of a stack of rectangular ($\frac{3}{4}\times2$ in.) foils arranged in the following order: 0.001-in. aluminum; 0.003-in. aluminum monitor; 0.001-in. aluminum guard; 0.010-in. tantalum target; 0.001-in. aluminum. The foils were aligned to superimpose exactly and bolted into a target holder with the aluminum monitor upstream from the tantalum. Two modifications of the above-described arrangement were also used: (1) When cross sections for products sensitive to secondaries (i.e., products with $Z\geqslant71$) were being measured, the two outside guard foils were omitted and a 0.001-in. tantalum foil (32 mg/cm²) was substituted for the

* Research performed under the auspices of the U. S. Atomic Energy Commission.

[1] J. M. Miller and J. Hudis, Ann. Rev. Nuclear Sci. **9**, 159 (1959).

[2] B. G. Harvey, *Progress in Nuclear Physics* (Butterworths-Springer, London, 1959), Vol. 7, p. 89.

[3] N. A. Perfilov, O. V. Lozhkin, and V. P. Shamov, Soviet Phys.—Uspekhi **3(60)**, 1 (1960).

[4] N. Metropolis, R. Bivins, M. Storm, A. Turkevich, J. M. Miller, and G. Friedlander, Phys. Rev. **110**, 185 (1958); N. Metropolis, R. Bivins, M. Storm, J. M. Miller, G. Friedlander, and A. Turkevich, Phys. Rev. **110**, 204 (1958); also, Dr. G. Friedlander graciously made available some unpublished results of the above calculations. (There are also several papers by other workers, for which see page 164 of reference 1.)

[5] I. Dostrovsky, P. Rabinowitz, and R. Bivins, Phys. Rev. **111**, 1659 (1958). (See also reference 1, page 169 for a list of papers by other authors.)

[6] G. Rudstam, Doctoral thesis, NP-6191, University of Uppsala, Uppsala, Sweden, 1956 (unpublished).

0.010-in. foil in order to reduce the mass per unit area of the stack; and (2) when cross sections for products with $A \leqslant 28$ were being measured, the 0.010-in. tantalum foil was flanked on both sides by 0.001-in. tantalum guard foils to absorb the recoil fragments in this mass range that originate in the aluminum.

The target material was commercially available, pure tantalum foil. Spectrographic analysis showed that there was no impurity present in sufficient amounts to interfere with any of the reported product yields. In fabricating the foils, all of the tantalum and aluminum foils which were to be used in about ten bombardments were clamped together in a single stack and carefully machined to congruency.

The magnitude of error introduced into the measured cross sections by small misalignments in the foils when they were assembled into targets was estimated using the following data[7]: (1) For a few targets the amount of misalignment of the leading edge was estimated using a microscope; (2) in two bombardments, the (nonuniform) distribution of the radioactivity induced in the foils was determined. From these data it was estimated that the error associated with misalignments of the foils should not have exceeded 5%.

Irradiations. All of the irradiations were carried out in the circulating beam of the Bevatron at the Lawrence Radiation Laboratory in Berkeley, California. The technique used was quite similar to one developed at Brookhaven National Laboratory for use with the Cosmotron.[8] Until the end of each radio-frequency acceleration period the target was held in a shielded position for protection from low-energy particles lost from the circulating beam during acceleration. A pneumatic ram then pushed the target into the vacuum chamber to a position slightly inside the orbit of the circulating protons. As the magnetic field continues to rise after the radio-frequency accelerating voltage has been cut off, the radii of the proton orbits decrease and the protons strike the target. Immediately after each pulse of irradiation, the pneumatic ram withdrew the target to its shielded position to await the next acceleration cycle.

Chemical procedures. After irradiation, the tantalum target foil was immersed in 25-ml of hot (steam bath), concentrated hydrofluoric acid into which had been measured milligram amounts of each of three to eight different carrier elements in appropriate chemical forms. By the cautious, dropwise addition of concentrated nitric acid, well-controlled dissolution of the tantalum metal was accomplished within about ten minutes. The excess nitric acid was destroyed by the addition of concentrated formic acid to the hot target solution, $\frac{1}{2}$ ml at a time, until the reaction was complete. The target solution was then cooled, and radiochemical purifications of the carriers were performed using appropriate adaptations of standard procedures.[7,9] The purified elements were finally precipitated from solution as appropriate chemical compounds, deposited uniformly[10] over a circular area 1.8 cm in diameter on small disks of filter paper, covered with 0.00025-in. Mylar film, and taped to aluminum cards, in order to make securely mounted samples suitable for routine measurements of their radiation intensities and decay rates. When these measurements were completed, the samples were chemically analyzed to determine the fraction of the original carrier element that had been recovered.

Measurement of radiations. The radioactive decay of each sample was observed with a calibrated,[11] end-window, aluminum-wall, methane-flow proportional counter until its radiation intensity became immeasurably feeble, or until time limitations forced a halt (usually after about one year). In addition, most of the samples were observed with a calibrated[11] gamma-ray spectrometer consisting of a 1-in.$\times$1.5-in. sodium iodide crystal optically coupled to a photomultiplier tube, the spectra being displayed with the aid of a 50-channel pulse-height analyzer. The gamma-ray spectrometer was used to follow the decay in intensity of emitted K x-rays in every sample for which $Z \geqslant 46$, and to measure the intensity of characteristic gamma rays for specific nuclides, when practicable.

Measurement of beam intensity. About one day after the end of bombardment, the 0.003-in. aluminum monitor foil was cut into rectangular sections with dimensions comparable to the diameter of the sample deposits, taped to aluminum cards in the same way as the samples and observed with the calibrated proportional counter to determine the yield of the $Al^{27}(p,3pn)Na^{24}$ reaction (the product Na^{24} was identified by means of its 15-hr half-life). This reaction was used to measure the total integrated beam intensity, assuming a cross section of 10.5 mb.[12] A subtractive correction was applied for Na^{24}

[7] A more thorough account of many details of this work, e.g., radiochemical procedures, counting techniques, resolution of decay curves, sources of cited radiation abundances, Rudstam-type surface fitting, etc., may be found in J. R. Grover, thesis, University of California Radiation Laboratory Report UCRL-3932, 1957 (unpublished).

[8] R. Wolfgang, E. W. Baker, A. A. Caretto, J. B. Cumming, G. Friedlander, and J. Hudis, Phys. Rev. **103**, 394 (1956).

[9] Monograph Series on the Radiochemistry of the Elements, Nuclear Science Series NAS-NS-3001 to NAS-NS-3058(?) issuance beginning Jan. 1960 by National Academy of Sciences, National Research Council, Committee on Nuclear Science, Subcommittee on Radiochemistry; Chairman: W. Wayne Meinke.

[10] G. Friedlander and J. W. Kennedy, *Nuclear and Radiochemistry* (John Wiley & Sons, Inc., New York, 1955), pp. 279–280.

[11] These calibrations were done by D. W. Barr (proportional counters and gamma-ray spectrometer), using a Na^{24} source of known disintegration rate, and by M. I. Kalkstein (gamma-ray spectrometer) using an Am^{241} source of known disintegration rate.

[12] This yalue has been used in most of the radiochemical work with the Berkeley Bevatron. There are as yet no accurate determinations of this cross section near 6 Gev, but 10.5 mb is certainly reasonable and probably not in error by more than 20%. See P. Benioff, Phys. Rev. **119**, 316 (1960), and N. Horwitz and J. J. Murray, Phys. Rev. **117**, 1361 (1960). However, due to more recent work, many workers now prefer a cross section nearer 9 mb; see J. B. Cumming, A. M. Poskanzer, and J. Hudis, Phys. Rev. Letters **6**. 484, 646 (1961).

TABLE I. Experimentally measured cross sections. The symbols are explained in the text.

Nuclide	Cross section (millibarns)	Measured radiations, with abundances used	Estimated accuracy	Remarks
Be^{7}	26±3	0.48γ, *12 G*	*B*	
Na^{22}	⩽1.1	β^+, *89 G*		b
Na^{24}	8.7±0.5	β^-	*B*	
Mg^{28}	2.5	β^-/β_d^-	*B*	
P^{32}	4.4±0.5	β^-	*B*	a
P^{33}	3.5±0.1	β^-	*B*	a, b
Ca^{45}	1.5	β^-	*C*	
Ca^{47}	0.3	β^-	*C*	
Mn^{52g}	0.8	β^+, *33 G*	*B*	
Mn^{54}	6.3	0.84γ, *100 G*	*C*	
Mn^{56}	2.0	β^-	*C*	b
Co^{55}	0.03	β^+, *66 M*	*B*	b
$Co^{58}(+Co^{56})$	1.4	0.80γ, *100 G*	*P*	c
$Co^{61}(+Co^{63})$	0.67	β^-	*B*	c
Ni^{57}	⩽0.02	β^+, *50 M*		
Ni^{65}	0.40	β^-	*B*	b
Ni^{66}	0.12	β^-/β_d^-	*B*	
Cu^{61}	1.0	β^+, *66 M*	*B*	
Cu^{64}	3.6±0.0	$\beta^+ + \beta^-$, *57 G*	*A*	
Cu^{67}	0.64±0.02	β^-	*A*	b
Zn^{62}	0.016	$\beta^+ + \beta_d^+$, *110 E*	*P*	a
Zn^{69m}	0.031	$\epsilon + \beta^-$, *113 G*	*P*	a, b
Se^{72}	0.74	β_d^+, *78 G*	*B*	
Se^{73g}	1.5	ϵ, *21 G*/β^+, *72 G*	*B*	b
Sr^{82}	3.2	β_d^+, *96 M*	*B*	f
Sr^{85m}	0.9	0.23γ, *84 G*	*C*	
Sr^{87m}	0.14	0.39γ, *78 G*	*C*	d
Zr^{88}	6.8±0.5	0.40γ, *97 G*	*B*	b
Zr^{89}	5.8±0.4 8.3±0.8	β^+, *30 M* 0.91γ, *99 G*	*B* *B*	f
Zr^{95}	<0.5	~0.74γ, *98 G*		
Mo^{90}	1.5±0.1	ϵ, *55 M*/β^+, *33 M*/ϵ_d, *18 M*/β_d^+, *33 M*	*C*	a
Mo^{93m}	1.4±0.1	ϵ, *70 M*	*C*	a, b
Mo^{99}	0.11±0.01 (3)	ϵ, *9 M*/β^-	*A*	
Pd^{100}	2.3	*K*, *65 E*/*K*$_d$, *65 G*	*B*	
Pd^{101}	5.1	*K*, *66 G*	*B*	
Pd^{103}	6.8±0.7	*K*, *78 M*	*B*	
$Ag^{103}+Ag^{104g}$	5.6±0.2	β^+, *31 M*	*B*	b, e
Ag^{105}	6.5	*K*, *80 G*	*B*	f
Ag^{106g}	0.9	*K*, *70 E*	*P*	
$Ag^{112}+Ag^{113}$	⩽0.04±0.01	β^-		
Cd^{107}	6.3±0.5 (3)	*K*, *105 G*	*A*	
Cd^{109}	7.9±0.9	*K*, *93 G*	*C*	f
Cd^{115g}	⩽0.004	β^-		
$Sb^{117}+Sb^{?}$	7.2	*K*, *80 G*	*B*	g, b
$Sb^{118g}+Sb^{?}$	1.0	*K*, *127 M*	*P*	g, b
Sb^{119}	0.25	*K*, *86 G*	*P*	f
Sb^{120m}	⩽0.5	*K*, *100 E*		
Sb^{122}	⩽0.027	β^-, *97 G*		
$Te^{116}+Te^{117}$	8.5±1.4	β^+, *64 M*	*B*	h, b
Te^{118}	8.6±0.6 (3)	β_d^+, *83 G*	*A*	
Te^{119g}	8.7 8.6	*K*$_d$, *86 G* 0.64γ, *90 M*	*B* *B*	
$Te^{118}+Te^{119m}$	7.8 <σ <14.0	*K*, *100* <Rad. Abund. <*180*		
Te^{119m}	<0.6	0.64γ, *90* ?		b
Te^{121g}	12.4	*K*, *73 M*	*B*	f
Te^{121m}	0.54	0.21γ, *91 G*	*B*	b
Cs^{131}	⩽0.5	*K*, *73 G*		
Ba^{125}	6.1	*K*+*K*$_d$, *89 G*/β_d^+, *82 G*	*C*	i
Ba^{128}	7.1±0.7 (4) 6.4±0.7 (3)	ϵ_d, *10 G*/β_d^+, *76 G* *K*+*K*$_d$, *114 G*	*A* *A*	
Ba^{129}	11.2	*K*$_d$, *126 M*	*C*	i
Ba^{131}	13.3±2.7 (4)	*K*, *94 G*/*K*$_d$, *73 G*	*B*	f, j
Ba^{131}	<2			f
Ba^{140}	<0.5	β^-		
Ce^{133}	>3.3	β^+, *<100*		
Ce^{134}	13.1±2.6	β_d^+, *44 G*	*C*	
Ce^{141}	<0.8	β^-		
Nd^{139}	42 ?	β^+, *10*/β_d^+, *6*	?	k
Nd^{140}	20.6±2.6 (3)	β_d^+, *53 G*	*A*	
Eu^{145}	12.2±3.4	*K*, *100 E* 0.89γ, *70 E*	*C*	l, r
Eu^{146}	4.2	0.74γ, *80 M*	*P*	f, m
Eu^{147}	17.7±2.6	*K*, *100 E*	*C*	f
Eu^{147}	5.0	*K*, *100 E*	*C*	f
Gd^{146}	18.6±0.1	*K*+*K*$_d$, *211 E* 0.63γ$_d$+0.74γ$_d$, *145 M*	*B*	n
Gd^{147}	15.3	*K*, *100 E*	*B*	o
Gd^{149}	19.3	*K*, *100 E*	*B*	l
Gd^{151}	⩽29.7 27.1±0.7	*K*, *87 M* 0.15γ, *6.5 M*/0.18γ, *2.8 M*	*C* *C*	p, q
Gd^{153}	19.5±1.6	0.10γ, *56 G*	*B*	f
Tb^{149}	9.6	3.95 Mev α particle, *10 M*	*B* ?	r
Er^{160}	25.3	*K*, *82 M*/*K*$_d$, *82 E*	*B*	f
Tm^{165}	24.7	*K*, *100 E*	*B*	b
Tm^{167}	27.3	*K*, *100 E*	*B*	
Tm^{168}	1.1	*K*, *97 M*	*C*	
$Lu^{169}+Lu^{170}$	28.8±1.9	*K*, *100 E*	*C*	f, s
$Lu^{171m}+Lu^{172}$	21.7±4.8	*K*, *100 E*	*C*	f
Hf^{171}	~13	*K*$_d$, *100 E*	*P*	
Hf^{173}	13.4±0.1	*K*, *97 G* 0.12γ, *110 G*	*C*	t
Hf^{175}	13.3±0.3 18.5±0.2	*K*, *97 M* 0.34γ, *86 G*	*C* *B*	t
Ta^{177}	14.7	*K*, *87 G*		
Ta^{179}	43	*K*, *40 G*		
$Ta^{175}+Ta^{176}+Ta^{180m}$	59±3	*K*, *79 M*		u
Ta^{180m}	38±18	β^-, *21 G*	*P*	
W^{177}	1.5±0.4	*K*, *100 E*	*P*	
W^{178}	2.2±0.1	*K*+*K*$_d$, *154 G*	*A*	v
W^{181}	<1.5	*K*, *37 G*		

[a] Resolution of components with similar half-lives was achieved by a least-squares calculation.

[b] It is not known whether this cross section is a chain yield or an independent yield.

[c] The formation cross sections for Co^{56} and Co^{63} are expected to be negligible.

[d] The 0.39-Mev gamma ray displays a two-component decay curve; $T_{\frac{1}{2}}$=2.6 hr and 35.5 hr.

[e] The positron abundance adopted for this mixture is a weighted average of the values 36% for Ag^{103} and 21% for Ag^{104g}.

[f] These cross sections are corrected to either completely cumulative or completely independent from measured cross sections that include only part of the chain yield. The corrections are usually small, depend on experimental data where possible, and otherwise depend on estimates of the parent cross sections derived from yield systematics such as are demonstrated by Fig. 8(b).

[g] The quoted *K* x-ray abundance is that appropriate for the known isotope in the mixture.

[h] The quoted positron abundance is a simple average of 57% for 15.5-min Sb^{116} (assumed to be populated 100% by the decay of Te^{116}) and 71% for Te^{117} (ignoring the 2.5% positron decay branch in 2.8-hr Sb^{117}).

[i] The relative contributions of Ba^{126} and Ba^{129} were determined with the aid of an experiment in which the 33-hr Cs^{129} daughter of Ba^{129} was chemically isolated and counted.

[j] Twelve-day Ba^{131} and its 10-day Cs^{131} daughter comprise a complex system which was resolved from the rest of the decay curve using a least-squares analysis.

[k] According to the Nuclear Data Sheets,[15] this activity may be misassigned.

[l] 1.0 mb was subtracted from the cross section for forming Eu^{145} and added to the cross section for forming Gd^{149}, to accord with the known 10% alpha-decay branching in the decay of 4-hr Tb^{149}.

[m] The 0.74-Mev gamma-ray photopeak forms a "shoulder" on the high-energy side of the prominent 0.65-Mev gamma-ray photopeak (present in both 5.8-day Eu^{145} and 4.4-day Eu^{146}); the resolution, and, therefore, also the cross section, is rather uncertain.

[n] Nine-minute Dy^{150} populates Gd^{146} by alpha decay and leads to an erroneously high cross section. Macfarlane [R. D. Macfarlane, University of California Radiation Laboratory Report UCRL-9566, 1961 (unpublished), p. 48] gives the alpha-decay branching ratio as 0.18, but no correction has been applied because the cross section for forming Dy^{150} is not known; probably about 1.5 mb should be subtracted from the cross section for forming Gd^{146}.

[o] The half-life assumed for Gd^{147} is 37 hr. This is the value observed by the author in subsequent (unpublished) work. The cross section should probably be reduced by about 0.5 mb to correct for alpha decay from 20-min Dy^{151} (branching ratio =0.062) [R. D. Macfarlane, University of California Radiation Laboratory Report UCRL-9566, 1961 (unpublished), p. 48], and the cross section for Gd^{151} correspondingly raised.

formed in the monitor foil by secondary particles [chiefly by the reaction $Al^{27}(n,\alpha)Na^{24}$ induced by neutrons with energies >6.5 Mev]. This correction was assumed to be about 3% per 100 mg/cm² of tantalum present in the target stack, based mainly on the experimental results of Hudis.[13]

Data reduction.[7] The radioactive decay curves of the samples were analyzed into components in order to separate the contributions from the different isotopes of the same element. Usually standard graphical techniques were used, but occasionally it was necessary to perform a least-squares analysis on the data when graphical means proved inadequate, e.g., when two components had similar half-lives, or when radioactive daughter activities "growing in" after radiochemical purification rendered graphical resolution impractical. For several nuclides which decay with the emission of well-resolved, easily measurable gamma rays of known abundance, the gamma rays were observed directly and it was not necessary to depend on the decay curve analysis.

To compute the disintegration rate at the end of the bombardment for each radioactive species detected, corrections were applied to the observed counting rates to account for the following: decay during the time elapsed between the measurement and the end of bombardment; decay during the bombardment; chemical yield of the radiochemical purification; counter geometry; and abundance of radiations being detected.[14,15] For beta emitters, which were observed with the proportional counter, additional corrections were applied for absorption in the sample cover and counter window,[16] self-absorption and self-scattering in the sample material,[17] and back-scattering from the filter paper, scotch tape, and aluminum card.[18] The correction for dead-time losses was negligible. For the gamma-ray and x-ray emitters, which were observed with the gamma-ray spectrometer, additional corrections were applied for absorption in the beryllium absorbers used to screen out energetic particles,[19] photopeak counting efficiency in the crystal,[20] escape peak losses,[21] and register dead-time losses (mechanical registers were used, for each of which the correction was about 7% per 100 register counts per min). Corrections were seldom applied for "coincidence-summing" effects, but it is thought very unlikely that this correction exceeded 6% at the largest solid angle subtended by the crystal (1.3π sr).

Finally, the beam intensity deduced from the Na^{24} activity in the Al monitor foils was used to convert the disintegration rates at the end of bombardment into cross sections.

EXPERIMENTAL RESULTS

Presentation of the Data

The experimentally measured cross sections are presented in column two of Table I. The indicated deviations refer to reproducibility only; they appear whenever replicate determinations were made and are simply the difference between the lowest and highest measured cross sections divided by the number of determinations (the number of determinations is indicated in parentheses, if there were more than two). Values appearing in boldface are independent yields, the others are chain yields.

Column four of Table I gives an estimate of the accuracy of each reported cross section, excluding the uncertainty associated with the monitor cross section (±20%). The letter "*A*" means that the cross section is probably accurate to within a factor 1.15, likewise "*B*" means a factor 1.25, "*C*" a factor 1.4, and "*P*" a factor 2; these figures are intended to correspond roughly to standard deviations of the mean.

[13] Seven measurements of this correction made by J. Hudis, at 2.2–3 Gev on targets from Al to Pb, and two independent determinations, one by O. A. Schaeffer and D. Fisher for an iron target at 3 Gev, and one from this work for a copper target at 6 Gev, were converted to a common basis (see below) and combined to make a plot of the magnitude of the correction versus mass number. A smooth curve drawn through the data passes through the following points: $A=25$, 1.0%; $A=50$, 2.0%; $A=77$, 2.9%; $A=105$, 3.3%; $A=170$, 3.5%; $A=210$, 3.5%. This curve gives the percent by which the amount of Na^{24} found in the monitor foil is increased beyond that induced by the incident proton beam via the reaction $Al^{27}(p,3pn)Na^{24}$ per 100 mg/cm² of target material of the cited mass number A, assuming: (1) a target of closely stacked foils whose width and length are much greater than its total thickness, (2) the monitor-foil is upstream from the target foil. The scatter of the points is such that eight of the nine fall within a factor 1.5 of the smooth curve.

[p] The half-life of 150-day Gd^{151} is not known accurately.

[q] If no correction is made in the *K* x-ray decay curve for the presence of the 120-day Eu^{149} daughter(?) of Gd^{149}, the cross section for the formation of Gd^{151} is 29.7 mb, in agreement with the value obtained from gamma-ray measurements. If the correction is applied, the resulting cross section is 17 mb.

[r] The cross section for the formation of Tb^{149} was measured by L. Winsberg, University of California Radiation Laboratory Report UCRL-8618, 1959 (unpublished), p. 53.

[s] This cross section is the sum of the independent yield for Lu^{170} and the chain yield (probably) for Lu^{169}.

[t] The reported cross section for Hf^{173} includes 0.3 times the formation cross section for Ta^{173}. Likewise, the cross section reported for Hf^{175} includes 0.1 times the cross section for Ta^{175}.

[u] These cross-section values differ by about a factor 2 from the corresponding values reported earlier in reference 7. Since it was suspected that the tantalum chemical yields upon which the earlier cross-section values were based were erroneous, the hotter of the two samples was recounted (it still contained a measurable amount of ~600-day Ta^{179}) and its chemical yield redetermined to provide a basis for correcting the earlier cross-section values.

[v] Crude calculations indicate that the production of tungsten isotopes by interactions of secondaries with the tantalum target would lead to apparent cross sections comparable to those reported here, even though the targets were relatively thin (32 mg/cm² of Ta plus 27 mg/cm² of Al).

[14] D. Strominger, J. M. Hollander, and G. T. Seaborg, Revs. Modern Phys. **30**, 585 (1958).

[15] K. Way, *Nuclear Data Sheets*, National Academy of Sciences (National Research Council, Washington, D. C., 1960).

[16] G. I. Gleason, J. D. Taylor, and D. L. Tabern, Nucleonics **8**, 12 (1951).

[17] W. E. Nervik and P. C. Stevenson, Nucleonics **10**, 18 (1952).

[18] For negative-beta particles; B. P. Burtt, Nucleonics **5**, 28 (1949). For positrons; see in addition H. Seliger, Phys. Rev. **78**, 491 (1950); **88**, 408 (1952).

[19] C. Davisson and R. Evans, Revs. Modern Phys. **24**, 79 (1952).

[20] M. I. Kalkstein and J. M. Hollander, University of California Radiation Laboratory Report UCRL-2764, 1954 (unpublished).

[21] P. Axel, Brookhaven National Laboratory Report BNL-271, 1953 (unpublished); Rev. Sci. Instr. **25**, 391 (1954).

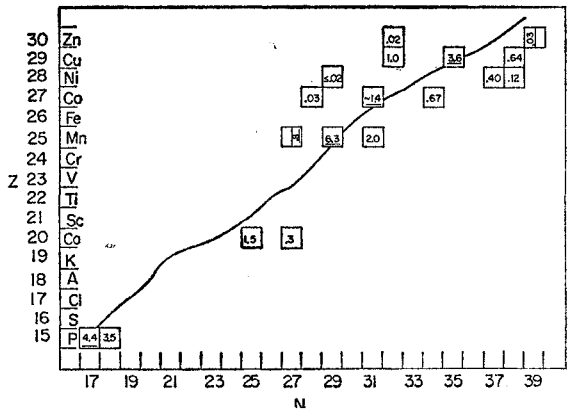

FIG. 1. Experimental cross sections (in millibarns) for the mass region $A=32$ to 69. In Figs. 1–5: independent cross sections are underlined; the unbroken curve represents the beta-stability line.

The reported cross sections depend critically on the abundances assumed for the particular types of radiations which were detected and measured. These radiation abundances are often somewhat uncertain. Therefore the radiations measured and the radiation abundances used[7] (together with estimates of their accuracy) are also listed in Table I, column three. The following is a description of the symbols employed. To the left of the comma is a symbol designating the type of radiation which was measured; β^+ for positrons, β^- for negatrons, ϵ for conversion electrons, γ for gamma rays (with a preceding number expressing the energy of the gamma ray in Mev), and K for K x rays. When measurements on the radiations from a daugher activity were important in establishing a cross section (e.g., from a daughter in secular equilibrium), the above symbols are given the subscript "d," as in K_d. To the right of the comma is an italicized number which gives the adopted radiation abundance, expressed in terms of the percent of the radioactive disintegrations. The letter immediately to the right of this number gives an estimate of its accuracy: G means $\pm 10\%$; M means either $\pm 20\%$, or in those cases where the decay abundances are calculated from decay scheme data,[7] that there are important uncertainties for which estimates are necessary (e.g., electron capture decay energies, gamma-ray multipolarities, allowedness or forbiddenness of positron decay, etc.); E means that the cited abundance is a guess, but few of the figures so labeled should be in error by more than 25%. If no radiation abundance is given it implies *100 G*. If, as often happens, several kinds or origins of radiation are important in determining a cross section, each one may be separately described, the different descriptions being separated by diagonals.

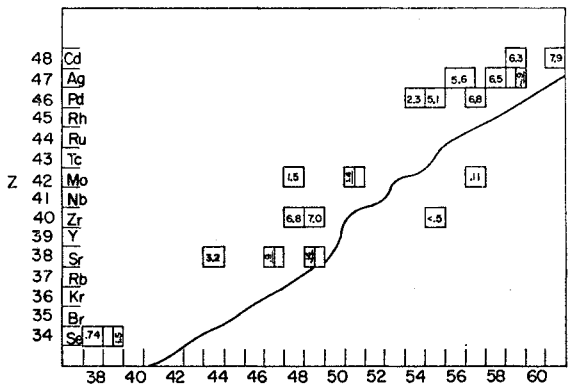

FIG. 2. Cross sections for the mass region $A=72$ to 109.

Empirical Description of the Data

To help see any pattern which may be contained in a set of measured cross sections such as is given in Table I, the values are customarily recorded on an N, Z grid (N is the number of neutrons, Z the number of protons in the product nucleus). Figures 1 to 5 represent such a plot, and the following paragraphs

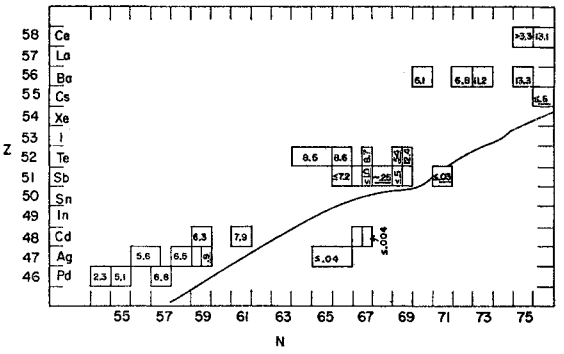

FIG. 3. Cross sections for the mass region $A=100$ to 134.

contain an empirical description of the features observed.

For product mass numbers $A=22$ to $A=67$, the cross sections are highest near the beta-stability line, becoming smaller rapidly as one goes to either neutron-excess or neutron-deficient isotopes.

For product mass numbers greater than $A\approx 72$, almost all of the products identified (nearly all of the products which were observed were identified) are neutron deficient. Upper limits are given for the formation cross sections of a few neutron-excessive products, and these all indicate small cross sections. There are a few data indicating that the independent cross sections on or near the beta-stability line are relatively small. The majority of the cross sections reported for neutron-deficient products represent chain yields, i.e., the observed product stands at the end of a relatively short-lived beta-decay chain so that the reported cross section really represents the sum of independent cross sections for all of the products included in the chain. Within any limited zone of

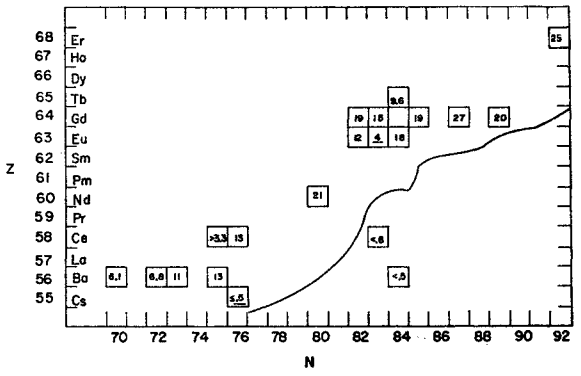

FIG. 4. Cross sections for the mass region $A=126$ to 160.

product mass numbers (e.g., $A=100$ to 109) those cumulative cross sections for neutron-deficient products nearest the beta-stability line are the largest, while those farthest away (i.e., most neutron deficient) are the smallest. Clearly, above mass $A\approx 90$ most of the reaction yield appears as neutron-deficient nuclides.

Mass Yield Distribution

Some of the data in Table I can be used to construct a mass yield curve, i.e., a plot of the total cross section summed over all reaction products at each mass number, σ_A, vs mass number A. There are a number of cumulative cross sections above mass number $A\approx 90$, such as those for Pd^{103}, Ba^{131}, Gd^{153}, Tm^{167}, etc. which can be seen from the above considerations to contain most of the total cross sections for their respective mass numbers; these data can therefore be entered on a mass yield plot with only small estimated corrections for the unmeasured parts of the total mass yields. Also, there are sufficient data around mass numbers 25 and 60 to permit estimates of unmeasured cross sections by short interpolations and thus to support estimates of the total mass yields near these points. The resulting plot is given in Fig. 6.

From Fig. 6 it is seen that all mass numbers below the target are represented with cross sections of at least several millibarns. The shape of the mass yield distribution is very similar to that resulting from the reactions of lead with 3-Gev protons,[8] but very different

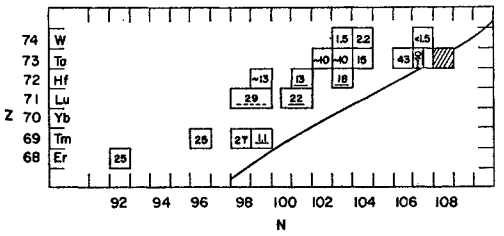

FIG. 5. Cross sections for the mass region $A=160$ to 181.

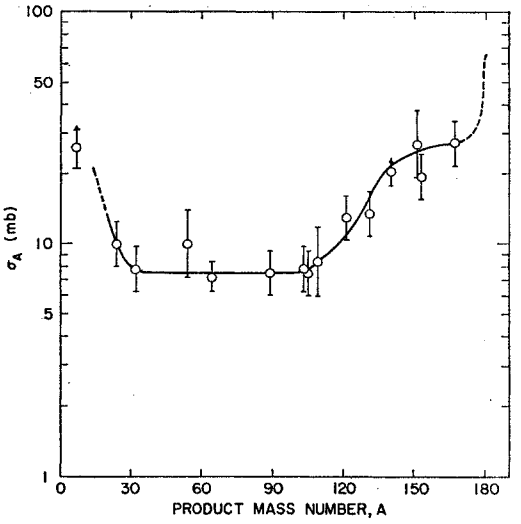

FIG. 6. Total mass yields versus product mass number.

from that resulting from the reactions of tantalum with 0.34-Gev protons[22] (Fig. 7).

Charge Distribution

The beta-stability line weaves back and forth somewhat as it proceeds through the N, Z plane, leading one to ask whether the cross sections show any obvious correlation with this phenomenon. Figures 8(a) and

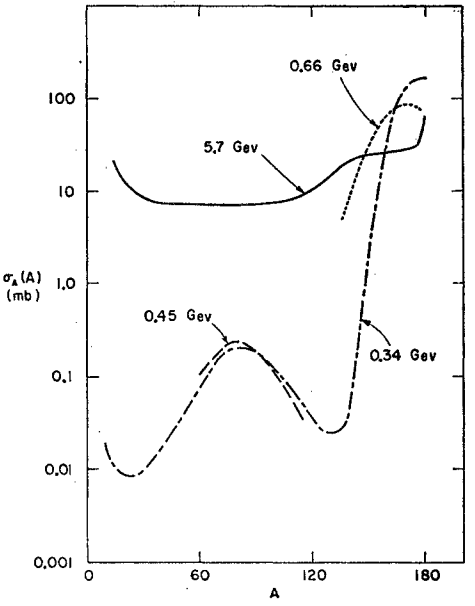

FIG. 7. Comparison of mass yield curves for the interactions of tantalum with high-energy protons. The curve at 0.34 Gev is from Nervik and Seaborg,[22] that at 0.45 Gev is from Kruger and Sugarman,[29] and that at 0.66 Gev is from A. K. Labrukhin and A. A. Pozdnyakov, Sov. J. Atomic Energy **7**, 862 (1961).

[22] W. E. Nervik and G. T. Seaborg, Phys. Rev. **97**, 1092 (1955).

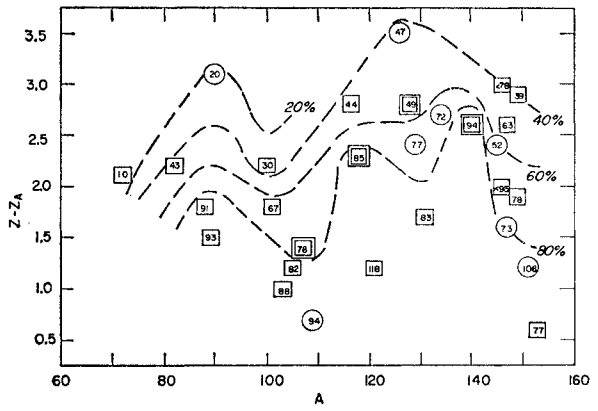

FIG. 8(a). Contour plot of $\sigma_c(A,Z)/\sigma_A$ in the coordinate system $Z-Z_A$ versus A (see text). In Fig. 8(a) and 8(b) the values plotted in double-boxes pertain to data having an accuracy classification of "A" in Table I, those in single boxes pertain to "B," and those in circles pertain to "C."

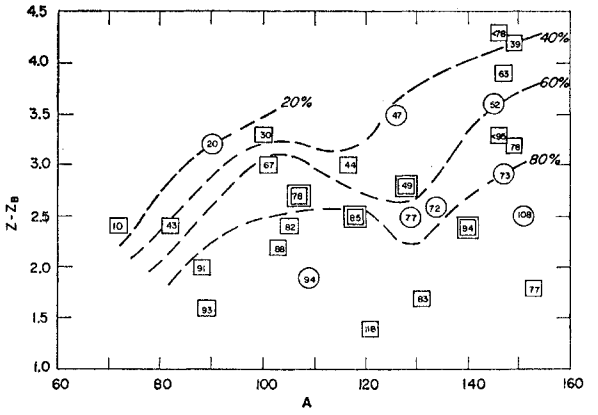

FIG. 8(b). Contour plot of $\sigma_c(A,Z)/\sigma_A$ in the coordinate system $Z-Z_B$ versus A (see text).

8(b) have been constructed in an effort to reveal such a relationship. In both figures, the abscissa is the product mass number A. In Fig. 8(a) the ordinate is the quantity $Z-Z_A$, where Z is the product atomic number, and Z_A is the most stable Z for a given mass number A. The values of Z_A used here are taken from Coryell,[23] and replace the twists and turns of the beta-stability line with discrete jumps which occur every time a major nucleon shell is filled. In Fig. 8(b) the ordinate is the quantity $Z-Z_B$, where Z_B is chosen from a smooth curve in the N,Z plane. This smooth curve is drawn in such a way that it follows the beta-stability line approximately, but does not reproduce its characteristic weavings (the curve used here is the locus of the most stable Z for a given A in the semi-empirical mass equation of Friedlander and Kennedy[24]). The numbers plotted in the boxes and circles are values of the ratio $\sigma_c(A,Z)/\sigma_A$ where $\sigma_c(A,Z)$ is the cumulative cross section for the neutron-deficient reaction product of mass number A and atomic number Z, and σ_A is the total product cross section at mass A interpolated from a smooth curve drawn through the points in Fig. 6 [the smooth curve is made to go above the point for Nd^{140} because Nd^{140} is too far from beta-stability for one to feel sure that the correction for unmeasured cross sections is small (see Fig. 4)]. Contour lines have been sketched in Figs. 8(a) and 8(b) to represent the approximate locus of lines of constant ratio.

The over-all impression gained from looking at either Fig. 8(a) or Fig. 8(b) is that the zone of products having the highest independent yields (i.e., the zone containing ratios between 0.25 and 0.75) tends to become increasingly neutron-deficient with increasing mass number. The contour lines appear smoother in Fig. 8(b) than they do in Fig. 8(a), which implies that the lack of smoothness of the beta-stability line is not strongly reflected in the cumulative cross sections. More is said about this topic in the discussion section.

The same systematic behavior of the data which encourages the use of contour lines in Figs. 8(a) and 8(b) also suggests that one might attempt to fit the data to a smooth (empirical) surface, as was done by Rudstam[6] for similar data. In the mass region $A=72$ to $A=153$ a smooth surface was determined[7] (ignoring the beta-stability line), the locus of which lies within $\pm 25\%$ of the measured cross sections for twenty-one of the twenty-five cumulative cross sections which were included in the fitting. Since most of the data are only accurate to within about $\pm 25\%$, one draws the interesting conclusion that the present data cannot exclude the possibility that the yield surface is "smooth" (and therefore that the lack of smoothness of the beta-stability line is not detectable in the data). Hence, also, the smaller features one might expect to see in the yield surface, such as effects connected with the evenness or oddness of product nucleon numbers, etc., may be obscured because of the limited accuracy and abundance of the data.

The approximate locus of the isobaric independent yield maxima $[Z_p(A)]$ can be inferred from the contours in Fig. 8(b), if it is assumed that the distributions have single, roughly symmetrical maxima.[25] The locus of these maxima in the N,Z plane is represented by the solid line in Fig. 9. Also included for comparison is the locus of the beta-stability line (dashed line) taken from the "G. E. Chart of Nuclides."

DISCUSSION

The description in the preceding section, of the observable patterns and systematics in the data, is

[23] C. D. Coryell, Ann. Rev. Nuclear Sci. **2**, 305 (1953).
[24] Reference 10, page 50.

[25] There is no evidence to expect other than a single maximum in the isobaric independent yield distribution, at a given mass number, for the reaction products of 6-Gev protons with tantalum. Measurements of the production of some Ba and Cs isotopes in the reactions of gold with 3-Gev protons lend some support to this view; see B. M. Gordon and L. Friedman, Phys. Rev. **108**, 1053 (1957).

almost completely empirical; little attempt is made to color the observations with ideas of their meaning. The problem of interpreting the observations in terms of nuclear structure and reaction mechanisms is explored in this section.

The distribution of products observed in high-energy nuclear reactions is currently explained in terms of appropriate combinations of the following four processes: (i) the initial high-energy cascade; (ii) the evaporation of nucleons and other more complex particles from excited nuclei; (iii) fission; and (iv) fragmentation. Processes (i) and (iv) are considered to take place in a shorter time scale ($\lesssim 10^{-21}$ sec) than processes (ii) and (iii), ($\gtrsim 10^{-20}$ sec), although it is recognized that a clean time-scale differentiation is somewhat unrealistic. (These four postulated processes and the histories of their origins are described in detail in several recent reviews,[1-3] in which they are also discussed in terms of the experimental evidence bearing on their validity, necessity, etc.) The following discussion of the data is given in terms of processes (i) to (iv), and is organized with respect to the two prominent aspects of the data already noted, (1) the mass yield distribution and (2) the charge distribution, as reflected in the locus of the isobaric independent yield maxima in the N, Z plane.

Interpretation of the Mass Yield Curve

Spallation and High-Energy Fission

For targets with mass numbers well below $A \approx 230$, the bulk of reaction products is expected to arise from spallation, which is the combination of processes (i) and (ii). For incident energies in the range 0.1 Gev $< E < 0.5$ Gev the spallation products form a characteristic mass yield distribution that displays a maximum for product mass numbers near the target and then decreases steadily and rapidly, often over several orders of magnitude, with decreasping product mass number. For target mass numbers and bombarding energies not too low (e.g., targets as heavy as silver and incident energies above about 0.3 Gev) a special zone of products is clearly distinguishable just below the spallation region which zone of products arises from high-energy fission,[26] i.e., a combination of processes (i), (ii), and (iii). In the mass yield curve, such a zone of fission products is usually characterized by a more or less distinct maximum appearing at a mass number somewhat smaller than half that of the target (for an illustration of the above-described features, see the 0.34-Gev curve in Fig. 7).

In looking at the mass yield curve in Fig. 6 with the usual idea of trying to identify one region due to spallation, and another due to fission, an ambiguity is apparent. The problem is especially clear if one looks only at the plotted points, ignoring the possibly misleading smooth curve. The "shoulder" near mass $A \approx 140$ can equally plausibly be exaggerated or suppressed (but not eliminated altogether, because the cross section for Nd^{140} should be relatively accurate) while the presence of a very shallow fission peak between $A \approx 50$ and $A \approx 100$ cannot be excluded. If the total mass yield distribution can truly be described as mainly the sum of a very broad spallation distribution and a very flat fission distribution, the two distributions overlap extensively. Since any subjective attempt to divide the mass yield distribution into zones (one in which spallation contributes more than half the yield at each mass number, and another in which fission contributes more than half) cannot help but be rather arbitrary, it is desirable to find some objective criterion which will help decide where the division should be made.

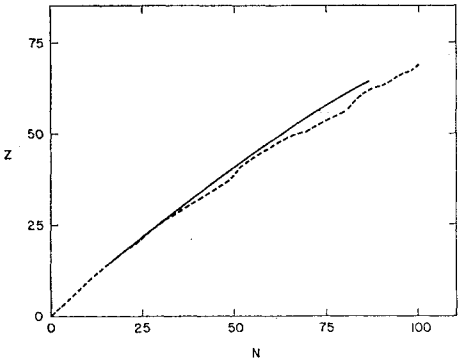

FIG. 9. Comparison of the experimentally-determined locus of isobaric independent yield maxima Z_p (solid line) with the beta-stability line (dashed line).

Such a criterion may be the occurrence of a zone of positive second derivative in the smoothed log mass yield curve (other than the expected toe-up at very low mass numbers and possible special effects very near the target mass). A justification for this proposed criterion is given in the Appendix. That there must be such a zone in the mass yield curve can be seen if one tries to draw through the points in Fig. 6 a smooth curve which does not have a zone of positive second differential. Such a curve cannot be drawn convincingly, and the zone of highest positive curvature is seen to occur somewhere between $A \approx 90$ and $A \approx 130$. This does not by itself indicate the presence of fission, it only indicates that in addition to spallation there is at least one more important process contributing reaction products; whether this process is fission is a problem requiring further experimental investigation. Evidence that fission is indeed an important contributor of products is provided by the nuclear emulsion data of Baker and Katcoff,[27] who report that 3% of the inter-

[26] Fission has been observed for targets as light as copper with incident proton energies as low as 60 Mev, but the cross sections are very small. See R. E. Batzel and G. T. Seaborg, Phys. Rev. **79**, 528 (1950).

[27] E. W. Baker and S. Katcoff, Phys. Rev. **123**, 641 (1961).

actions of 1-Gev protons and 11% of the interactions of 3-Gev protons with Ag and Br nuclei lead to fission. If the other process(es) gives a product distribution similar to that expected for fission, the point of highest positive second differential would provide a rough indication of the mass region where the unknown process and spallation give products with comparable probability; unfortunately there are not enough data to determine this point.

Emitted Light Particles

The emitted nucleons and light nuclei resulting from processes (i) and (ii) would be expected to appear in the mass yield curve as a steep increase at the smallest mass numbers. The cross section for the production of Be^7 is the only datum in this region; it seems to be appropriately high.

Fragmentation

There is not much evidence in Table I bearing on the proposed fragmentation process[3,8] (iv). The product mass region most sensitive to this mechanism lies between $A\approx15$ and $A\approx40$, in which the only data are the cross sections for Na^{24}, Mg^{28}, P^{32}, P^{33}, and an upper limit for Na^{22}. These data were used, with plausible estimates for unmeasured cross sections, to obtain a higher total mass yield at $A=24$ (10 mb) than at $A=32$ (7.8 mb). These cross sections seem to be too high for the products to be particles emitted in processes (i) and (ii), while if they are fission products, one might not expect the mass yield at $A=24$ to be higher than that at $A=32$. However, the effect is too small compared to the uncertainties, both in the data and in the estimates of unmeasured cross sections, to be taken as real evidence for fragmentation as an important source of these products. The product nuclei complementary to these "fragments" would probably lie roughly in the mass region $A\sim130$ to $A\sim160$, where their contribution is not obviously discernible because of the overwhelming preponderance of spallation products.

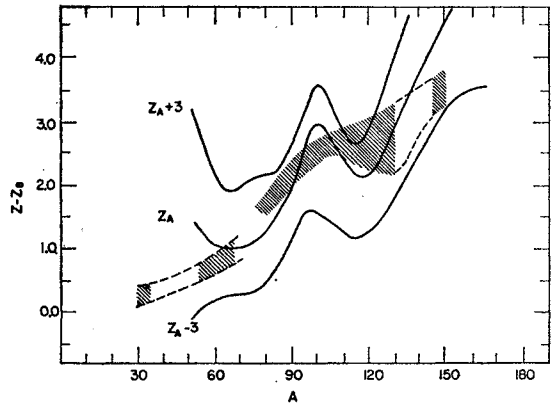

FIG. 10. Comparison of the locus of isobaric independent yield maxima Z_p with the calculated[6] locus of the mean evaporation products for nuclei excited to a nuclear temperature of 4 Mev (see text).

Total Cross Section

The total inelastic cross section for the interaction of tantalum with 5.7-Gev protons cannot be ascertained with accuracy from the reported data. One does not know, as already mentioned, whether or not products in the mass region $30\lesssim A\lesssim110$ (or higher) arise to an important degree from a binary (or multiple) process such as fission. Also, most of the estimated total inelastic cross section depends on only six points at product mass numbers above $A\approx120$, so that most of the data reported in this paper do not enter into the calculation (except indirectly by assuring the plausibility of those numbers which are used). With such reservations in mind, the smoothed mass yield curve of Fig. 6 was summed from $A=71$ to $A=180$ to obtain 1.8 b (or 1.5 b if the monitor cross section is taken to be 9.0 mb instead of 10.5 mb; see reference 12). For comparison, the prescription of Atkinson *et al.*[28] was used to calculate the reaction cross section for 5-Gev neutrons incident on tantalum; the result was 1.52 b. Therefore 1.8 b is an acceptable figure, and provides assurance that the six cross sections which were used to estimate the mass yield curve above $A\approx120$ are reasonable in magnitude.

Assuming that a rough estimate of the "fission" cross section is obtained from an integration under the smooth curve of Fig. 6 between $A=30$ and 110, one finds 0.3 b for a binary process. This is about 15 to 20% of the total cross section, a value consistent with Baker and Katcoff's[27] (previously mentioned) value of 11% for the interactions of 3-Gev protons with AgBr.

Interpretation of the Isobaric Independent Yield Maxima (Z_p) Curve

Qualitative Features Expected for the Charge Distribution of Evaporation Progenitors

In interpreting the Z_p curve, it is helpful to have at hand a knowledge of whatever qualitative features of the distribution of evaporation progenitors with respect to A, Z, and excitation energy are reasonable within the current state-of-knowledge of high-energy nuclear reactions. These features may be summarized as follows.

Spallation. In the spallation region, most of which appears to lie above $A\approx130$, it is plausible to assume that the bulk of the evaporation progenitors are neutron-deficient, that they possess a broad spectrum of excitation energies, and that their average excitation energies are very large, of the order of hundreds of Mev. These predictions are made by Metropolis *et al.*[4] with the help of their Monte Carlo calculations of the

[28] J. H. Atkinson, W. N. Hess, V. Perez-Mendez, and R. Wallace, Phys. Rev. 123, 1850 (1961).

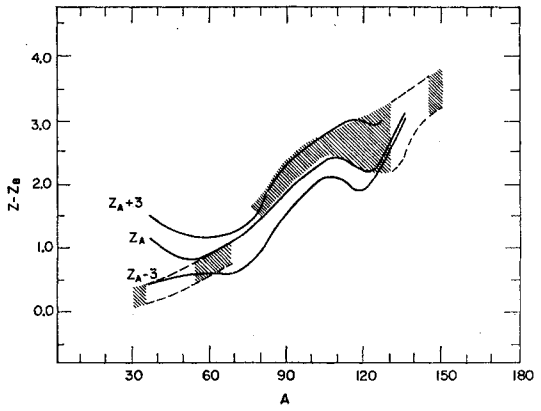

FIG. 11. Comparison of Z_p with the calculated locus of the mean evaporation products[5] for nuclei excited to a nuclear temperature of 6 Mev (see text).

high-energy cascade process (although the highest bombarding energy they considered was 1.8 Gev).

Fission. It is not as easy to make plausible guesses about the charge and energy distributions of the fission products as it is for the cascade products. Also, a special problem arises because one does not know whether the fission products are themselves highly excited evaporation progenitors. Unfortunately, there is as yet no convincing theory which can be used as a guide, even for bombarding energies in the range $0.1\ \text{Gev} \lesssim E \lesssim 0.5\ \text{Gev}$ where there are more data.[29] Furthermore, the striking change that occurs in the characteristic appearance of the "fission product" region (i.e., the middle mass region where $30 \lesssim A \lesssim 120$) in the mass yield curves of lead[8] and tantalum (Fig. 7) when the bombarding energy is increased from a few hundred Mev to a few Gev is a warning that even a theory good for bombarding energies of a few hundred Mev may become inadequate at Gev energies. In the absence of definite knowledge, the interpretation of the Z_p curve is attempted using the plausible assumption that the evaporation progenitors for products appearing in the middle mass region are highly excited and evaporate many particles.[29]

In the following section an attempt is made to see what information can be extracted from the data that will help determine the charge distribution of evaporation progenitors. For this it is necessary to have a quantitative knowledge of how the evaporation of nucleons and other particles from the highly excited nuclei changes the original distribution of evaporation progenitors into the observed distribution of reaction products. The mathematical problem of particle evaporation from highly excited nuclei has been treated by several workers, but probably most thoroughly and with the fewest simplifying approximations by Dostrovsky, Rabinowitz, and Bivins[5] (DRB), who used a fast electronic computer and Monte Carlo techniques. Throughout the following discussion it is assumed that nuclear evaporation theory is applicable, even for excitation energies of several hundred Mev (where there is doubt of its validity[5]).

Comparison of the Data with the Calculations of DRB

A comparison of the results of the calculations of DRB with the experimental data is given in Figs. 10 to 12. In each figure, the shaded zones indicate the approximate locus of the Z_p curve, wherever there seem to be enough data to permit an estimate. Above $A \sim 80$ the shaded zones correspond to the region between the contour lines $\sigma_c(A,Z)/\sigma_A = 40\%$ and 60% in a plot such as Fig. 8(b). Ideally one would choose the contour line for 50% to represent Z_p; however the above choice of upper and lower limits serves as a reminder that the average experimental accuracy is about $\pm 25\%$. The ordinate scale was reduced by 0.5 units of Z in transferring contour lines from Fig. 8(b) to Figs. 10 to 12 because the experimental (cumulative) cross sections are for whole-integer values of Z. The shaded zones are actually wider than the distance between the 40% and 60% contour lines in Fig. 8(b) because an attempt was made to include the effect of the ambiguity in drawing the smoothed mass yield curve. A contour plot similar to Fig. 8(b) was prepared using the mass yield curve derived from a Rudstam-type surface-fitting procedure.[6,7] This mass yield curve was drawn quite independently of the one in Fig. 6, makes use of more of the data, and depends on a different way of correcting for unmeasured cross sections. The resulting 40% and 60% contour lines did not coincide perfectly with the corresponding lines in Fig. 8(b), and, therefore, the shaded zones in Figs. 10 to 12 were drawn wide enough to encompass both of the 40% to 60% zones simul-

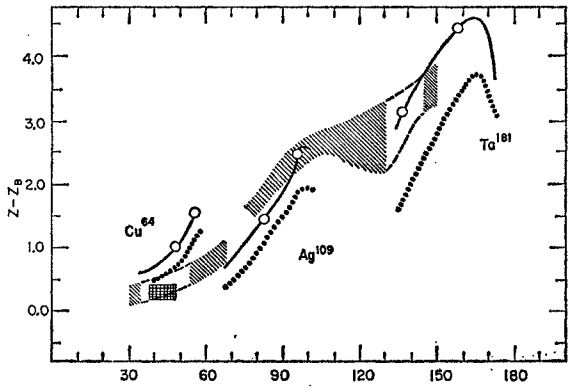

FIG. 12. Comparison of Z_p with the calculated locus of the mean evaporation products for Cu^{64} excited to energies from 100–500 Mev, and Ag^{109} and Ta^{181} excited to energies from 100 to 700 Mev, for $a = 0.1A$ Mev^{-1} (solid lines) and $a = 0.05A$ Mev^{-1} (dotted lines). (See text.)

[29] For discussions of this matter see: P. Kruger and N. Sugarman, Phys. Rev. **99**, 1459 (1955); N. T. Porile and N. Sugarman, Phys. Rev. **107**, 1410, 1422 (1957); P. K. Kofstad, University of California Radiation Laboratory Report UCRL-2265, 1953 (unpublished); reference 1, p. 182; and refereenc 3, p. 31.

taneously. Below $A \approx 70$, the shaded zones were taken from a Rudstam-type surface-fitting procedure which was applied to the data in this region, but one would draw almost identical zones directly from an inspection of Fig. 1.

The solid curves in Figs. 10 and 11 are taken from the results given in Figs. 9 and 10 of the paper by DRB, and represent the calculated locus of the mean mass and atomic number of the final products resulting from the de-excitation of selected nuclei (i.e., synthetic evaporation progenitors) by evaporation of nucleons and other particles. A state density parameter of the form $a=0.1A$ Mev^{-1} was employed, where the dependence of the nuclear state density $\rho(E)$ on excitation energy E was assumed to be

$$\rho(E) = (\text{const}) \exp[2(aE)^{\frac{1}{2}}]. \quad (1)$$

No correction was applied to take account of the depression of the Coulomb barrier arising from nuclear excitation. The three solid curves in each figure correspond to three assumed groups of synthetic evaporation progenitors, which differ from each other by their proximity to the beta-stability line. Those that lie along the beta-stability line are labeled by Z_A; those that lie three Z units in excess of, or deficient of the most stable Z at each A are labeled by Z_A+3 and Z_A-3, respectively. In Fig. 10, the synthetic evaporation progenitors (irrespective of their mass numbers) possessed excitation energies E such that $t=4$ Mev, as calculated from the relation $E=at^2$. In Fig. 11 the corresponding value is $t=6$ Mev.

From both Figs. 10 and 11 it is at once apparent that the over-all trend of the Z_p curve toward increasing neutron deficiency with increasing product mass number is well duplicated by the calculation. This trend is, of course, due to the effect of the Coulomb barrier in decreasing the emission rate of charged particles relative to neutrons. The results of the $t=6$ Mev calculation seem to follow the shaded zones somewhat better than the results of the $t=4$ Mev calculation, and one might tentatively conclude that the data are consistent with the view that in the mass region from $A \approx 80$ to $A \approx 135$ there is extensive evaporation from a distribution of evaporation progenitors which is itself somewhat neutron deficient. That one's impression that the "fit is better" for the $t=6$ Mev curves than for the $t=4$ Mev curves is not illusory is made more convincing if the calculated curves are plotted directly on Fig. 8(b). However, there is no good reason to believe that the evaporation progenitors display an initial constant temperature throughout such a broad range of mass numbers; indeed the calculations of Metropolis *et al.*[4] provide a convincing argument that the evaporation progenitors possess a wide distribution of excitation energies. The above observation should be construed to mean that the average excitation energies must be substantially above the values which would give $t=4$ Mev. It is of interest in this connection to mention that, for $t=6$ Mev, products appearing in the mass region $A=80$ to 135 would correspond to progenitors in the mass region $A \approx 105$ to 180 (on the average), while for $t=4$ Mev the same product mass range corresponds to progenitors in the mass region $A \approx 90$ to 155, according to DRB's calculations.

Also manifest is the tendency for the mean products from the three assumed types of synthetic evaporation progenitor to converge toward the same line with increasingly extensive evaporation (as has previously been pointed out by Halpern *et al.*).[30] At $t=6$ Mev the calculated curves are not widely separated, averaging less than one-half Z unit apart, even though the synthetic evaporation progenitors are separated by three Z units. This means that as long as there is extensive evaporation, the appearance of fission as a mechanism for producing the evaporation progenitors will not be strongly reflected in the positions of the isobaric independent yield maxima, even if the neutron deficiency of the fission-originated progenitors is very different from that of the cascade-originated progenitors. If one inspects Figs. 10 and 11 for evidence of a changeover from predominantly cascade-originated progenitors to predominantly fission-originated progenitors (from the evidence provided by the mass yield curve, one is led to look around $A \approx 110$), it is clear that no unequivocal statement can be made. Perhaps a very large difference (e.g., five Z units) between the two types of progenitors would be detected, but differences as large as two Z units would be completely swallowed up in the experimental errors and interpretational uncertainties.

In both figures, minima appear in the calculated curves around $A \approx 70$ and $A \approx 120$. Unfortunately these minima occur in just the regions where the data are scantiest. Other than to assert that the cross section for the production of Ba^{128} should be one of the firmest in the whole set (it is this cross section which causes most of the dip in the 0.6 contour near $A \approx 130$), and that it is considered more trustworthy than the cross section for Ba^{126}, nothing can definitely be said about whether these features are observable in the data. These predicted minima are due to the influence of the major nucleon shells (see DRB); it is interesting to see how differently the major shells are reflected in the calculated results than is implied in the naive surmise that led to the construction of Fig. 8(a).

Below $A \approx 70$, it appears, on the basis of the comparison with DRB's calculations, that the evaporation precursors are neutron excessive, irrespective of whether or not there is extensive nucleon evaporation. This is the same conclusion as that reached by Wolfgang *et al.*[8] in their study of the reactions of lead with 3-Gev protons, and comprises part of the evidence for their

[30] I. Halpern, R. J. Debs, J. T. Eisinger, A. W. Fairhall, and H. G. Richter, Phys. Rev. **97**, 1327 (1955).

proposed fragmentation mechanism. In the mass region $A=38$ to 48, Friedlander and Yaffe[31] measured several cross sections for products arising from the interactions of lead with 3-Gev protons; an approximate Z_p locus was estimated from their results and is plotted in Fig. 12 as a cross-hatched zone, to compare with the results of this study.

It should be emphasized at this point that the plotted curves derived from DRB's calculations do *not* represent the results of attempted calculations of the Z_p curve starting with assumed distributions of synthetic evaporation progenitors. The calculated "predictions" of DRB are being used only in qualitative comparisons with the experimental data; any conclusions must be drawn cautiously, with an awareness of the serious qualifications enforced by the interacting effects of the unknown distributions in excitation energy, A, and Z of the evaporation progenitors.

The effect, on the calculated product distribution, of varying the parameter a was also investigated by DRB. Contradictory results have been obtained[32] in various attempts to measure a, and it is interesting to see if any information regarding it can be extracted from the experimental data of this report. DRB calculated the locus of mean evaporation products for the nuclei Ag^{109} and Ta^{181} initially excited to energies of 100 to 700 Mev (in steps of 100 Mev), and likewise for Cu^{64} from 100 to 400 or 500 Mev. Their calculation was performed for the two assumptions $a=0.1A$ Mev^{-1} and $a=0.05A$ Mev^{-1}, which give the mass-dependence, and the upper and lower extremes of magnitude most commonly accepted for a (but do not include the effects expected near closed nucleon shells).[33] The mean evaporation product distributions calculated by DRB are plotted[34] in Fig. 12. One sees that the change effected in the course of a calculated mean product line, when a is changed from $0.1A$ Mev^{-1} (solid lines) to $0.05A$ Mev^{-1} (dotted lines), is about the same as that brought about by a change of Z in the synthetic evaporation progenitors of two to four units, or by a change in t from 4 Mev to 6 Mev.[35] All of these changes are comparable with the indicated inaccuracy in the experimental determination of the Z_p curve. The effects of the various relevant factors are so interdependent that even when more accurate experimental work is done, it will probably not be possible to extract unambiguous information on any one of them without knowing the others.

A useful result of the foregoing discussion is that it pinpoints specific information that cannot be unambiguously obtained from the present experiment, but that might still be sought via other experiments on this same target-projectile system. For example, some of the desired additional information on a could probably be obtained by measurements of the spectra of emitted particles. Also, information on the distribution of excitation energy in the evaporation (or fission) progenitors, or on the relative contributions from fission and spallation in the middle mass region, might be sought through measurements of the recoil ranges and angular distributions of selected products.

The following list of statements summarizes the results of this discussion:

I. There are at least two important mechanisms contributing reaction products. Whether there are more than two cannot be ascertained from the data of this report. One of the mechanisms, presumably spallation, contributes mainly products having mass numbers above $A\approx120$, while the other(s) (fission?) makes its most observable contribution for product mass numbers less than $A\approx120$.

II. The over-all trend of the highest isobaric independent yields toward increasing neutron deficiency with increasing mass number, which is caused by the effect of the Coulomb barrier, is well reproduced in the calculations of Dostrovsky, Rabinowitz, and Bivins.

III. There are not enough data to confirm or contradict the interesting structure predicted by DRB's calculated mean-product lines (i.e., the maxima and minima in Figs. 10 and 11).

IV. In the formation of products between mass numbers $A\approx80$ and $A\approx150$ most of the evaporation progenitors are not extremely neutron excessive or deficient (although whether they are mildly one or the other cannot be ascertained), and extensive evaporation has probably taken place.

V. In the formation of products below mass number $A\approx60$, most of the evaporation progenitors were probably neutron excessive, but it cannot be ascertained whether or not there was a large amount of evaporation.

VI. The results do not contradict the postulate, made earlier, that the products appearing in the "fission product" region are the result of extensive particle evaporation from highly excited progenitors.

VII. The results are consistent with both $a=0.1A$ Mev^{-1} and $a=0.05A$ Mev^{-1}, although if, in the region above $A\approx80$, one postulates (very reasonably) that the evaporation progenitors are neutron deficient and excited to average temperatures of the order of $t=6$ Mev or higher, $a=0.1A$ seems to be somewhat favored over $a=0.05A$.

---

[31] G. Friedlander and L. Yaffe, Phys. Rev. **117**, 578 (1960).
[32] G. Igo and H. Wegner, Phys. Rev. **102**, 1364 (1956).
[33] T. D. Newton, Can. J. Phys. **34**, 804 (1956).
[34] The open circles represent the interpolated positions for $t=4$ Mev and $t=6$ Mev, and when compared with the corresponding points in Figs. 10 and 11 serve as a convenient check on the accuracy with which the graphs in DRB's paper can be read.
[35] DRB also investigated the effect of an assumed dependence of the Coulomb barrier on excitation energy. The resulting calculated mean product curves for $a=0.1A$ Mev^{-1} are similar to the corresponding curves already plotted in Fig. 12; the effect is somewhat smaller than that brought about by the above described change in a.

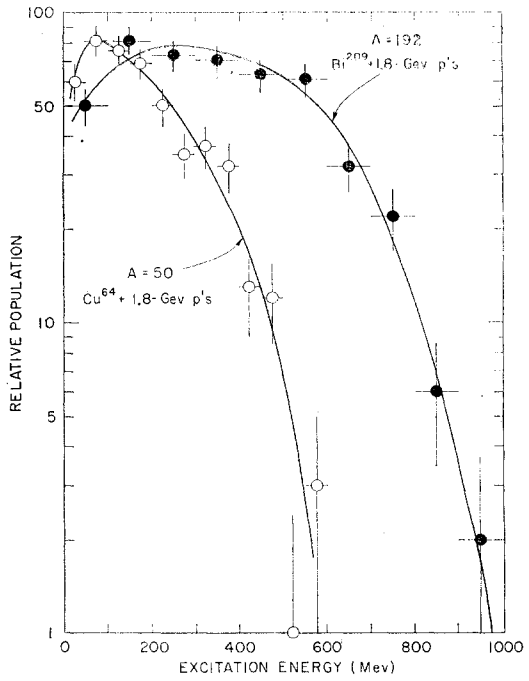

FIG. 13. Semilog plot of the calculated excitation energy distribution[4] at $A=50$ resulting from the bombardment of Cu^{64} with 1.8-Gev protons (open circles), and at $A=192$ resulting from the bombardment of Bi^{209} with 1.8-Gev protons (closed circles). (See text.)

ACKNOWLEDGMENTS

I wish to express my gratitude to Professor G. T. Seaborg, under whose direction this work was initiated and performed, and to Dr. E. K. Hyde for his considerable guidance and advice. The able assistance of Dr. E. Huffman and his staff in performing the many chemical analyses of the final precipitates of the radiochemical purifications, and of G. Shalimov in performing many spectrographic analyses is gratefully acknowledged. Dr. J. Hudis, Dr. O. A. Schaeffer, and Professor D. Fisher were most gracious in permitting me to use their unpublished measurements of the correction of the monitor response for secondaries. Valuable encouragement, discussion and criticism has been contributed by Dr. G. Friedlander, Professor A. A. Caretto, Dr. R. H. Shudde, and Dr. L. Winsberg.

APPENDIX

For a smooth curve drawn through a plot of $\log\bar{\sigma}_A$ versus A, one expects to find (as an over-all trend) that $d^2\log\bar{\sigma}_A/dA^2<0$ provided the mass yields $\bar{\sigma}_A$ arise entirely from high-energy spallation. The following argument advanced for the justification of this view is based on calculated distributions of excitation energies in the nuclei remaining from the high-energy cascade process.

The excitation energy spectra pertinent to the argument of this Appendix are not those of the primary cascade products themselves but rather are those of nuclei having mass numbers sufficiently smaller than that of the target nucleus that they are not themselves formed to any important extent as primary cascade products. They are formed instead by particle evaporation from the primary cascade products, and in general go on to evaporate more particles. Two calculated examples of the excitation energy spectra of such nuclei are shown in Fig. 13. One example is for the interactions of Cu^{64} with 1.8-Gev protons, evaluated for an "average" nucleus (see below) with $A=50$; the other is for the interactions of Bi^{209} with 1.8-Gev protons, evaluated at $A=192$. These examples were both calculated, with the help of Eq. (A11) (see reference 36), from the distributions in mass, nuclear charge, and excitation energy resulting from the initial high-energy cascade process, as calculated by Metropolis *et al.*[4] The mass numbers chosen for the examples (i.e., 50 and 192) were in each case the highest possible, consistent with the above-described restriction.

For each of the examples in Fig. 13, one observes that the second derivative with respect to the excitation energy, of the logarithm of the smooth curve drawn through the points, is less than zero over the entire curve. One expects this property of the excitation energy spectra to be reflected in the corresponding property $d^2\log\bar{\sigma}_A/dA^2<0$. The details of an argument supporting this statement are presented in the following paragraphs.

Let $p(A,Z,E)$ be the distribution of excitation energy E in a nucleus of mass number A and atomic number Z. Let α represent the highest mass number below which there is no important direct contribution to $p(A,Z,E)$ from the cascade process; for $A<\alpha$ then, $p(A,Z,E)$ is the combined result of particle evaporation from many different cascade products with $A\geqslant\alpha$.

The influence of nuclear charge is of secondary importance when only the mass yield curve is of interest, so to eliminate the argument Z from further consideration it is convenient to define another excitation energy distribution $P_A(E)$ as the appropriately weighted sum of the $p(A,Z,E)$ for all Z at each A,

$$P_A(E)=\sum_Z C(A,Z)p(A,Z,E), \qquad \text{(A1)}$$

where the coefficients $C(A,Z)$ are the weighting factors [the two curves in Fig. 13 are examples of $P_A(E)$ evaluated at $A=\alpha-1$].

The transformation of $P_A(E)$ into $P_{A-1}(E)$ to be associated with the evaporation of a nucleon (the evaporation of particles more massive than nucleons is neglected) is

$$P_{A-1}(E)\approx\int_E^{E_{m(A)-B}} S_A(E,x-E)P_A(x+B)dx, \qquad \text{(A2)}$$

where the normalized energy spectrum of the evaporated nucleons is $S_A(E,\epsilon)$. The symbol ϵ is related to

the evaporated nucleon energy by the demand that the amount of nuclear de-excitation resulting from a nucleon evaporation be $B+\epsilon$, where B is a suitable "effective" nucleon binding energy. For nuclei of a given A, the parameter B is approximately the appropriately weighted average of (i) the neutron binding energies; and (ii) the proton binding energies plus Coulomb barriers. For the argument given here, it is sufficiently accurate to regard B as a constant independent of A; its value is expected to be around 10 Mev. The maximum excitation energy at mass number A is symbolized by $E_m(A)$, so that $P_A(E)=0$ for $E>E_m(A)$.

The shape of the spectrum $S_A(E,\epsilon)$ requires that most evaporated nucleons possess an energy such that ϵ is not more than a few Mev different from the average energy $\tilde{\epsilon}$, where (for medium to heavy nuclei) $\tilde{\epsilon}$ is crudely comparable to or somewhat larger than B at high values of $E+\epsilon$ (hundreds of Mev) and smaller than B at low values of $E+\epsilon$ (tens of Mev). The emission energy spectrum is thus a relatively sharply peaked function when seen on the scale of the excitation energy spectrum, so that it is a reasonable first approximation to replace $S_A(E,\epsilon)$ with a delta function

$$S_A(E,\epsilon)=\delta(\epsilon-\tilde{\epsilon}). \tag{A3}$$

From Eq. (1) one obtains $\tilde{\epsilon}\approx 2[(E+\epsilon)/a]^{\frac{1}{2}}$. Substitution of (A3) into (A2) and evaluation of the integral gives, for $E>B$,

$$P_{A-1}(E)=[1+(1+aE)^{-\frac{1}{2}}]\times P_A\left(E+B+\frac{2}{a}\{1+(1+aE)^{\frac{1}{2}}\}\right). \tag{A4}$$

The argument of the P_A function in Eq. (A4) is conveniently interpreted in the following way. According to the delta-function approximation of Eq. (A3), there is for every combination of A and E a corresponding "average emission energy" $\tilde{\epsilon}(A,E)=\tilde{\epsilon}\approx 2[(E+\tilde{\epsilon})/a]^{\frac{1}{2}}$. With some algebraic manipulation one finds $\tilde{\epsilon}\approx(2/a)(1+[1+aE]^{\frac{1}{2}})$. The energy $\tilde{\epsilon}$ may also be regarded as the average energy of the nucleons emitted from a nucleus of mass number A having an excitation energy of $E+B+\tilde{\epsilon}$. Thus, in terms of $\tilde{\epsilon}$, Eq. (A4) becomes

$$P_{A-1}(E)\cong(1+\tilde{\epsilon}/E)^{\frac{1}{2}}P_A(E+B+\tilde{\epsilon}). \tag{A5}$$

The approximation $(1+aE)^{\frac{1}{2}}\approx(aE)^{\frac{1}{2}}$ has been used to derive the factor $(1+\tilde{\epsilon}/E)^{\frac{1}{2}}$ on the right side of Eq. (A5).

The calculation of $\bar{\sigma}_{A-1}$ (apart from an arbitrary constant factor) can be performed using the following expression, which circumvents the difficulty that Eq. (A4) cannot be used for $E<B$:

$$\bar{\sigma}_{A-1}=\int_B^{E_m(A)}P_A(E)dE-\int_B^{E_m(A)-B}P_{A-1}(E)dE. \tag{A6}$$

Insertion of Eq. (A4) into (A6) gives

$$\bar{\sigma}_{A-1}=\int_B^{2B+\tilde{\epsilon}(A-1,B)}P_A(E)dE, \tag{A7}$$

which generalizes to

$$\bar{\sigma}_{A-j}=\int_{E_j}^{E_{j+1}}P_A(E)dE, \tag{A8}$$

where $j=1, 2, 3, \cdots$ and where the first few E_j are

$$\begin{aligned}
&E_1=B,\\
&E_2=2B+\tilde{\epsilon}(A-1,B),\\
&E_3=3B+\tilde{\epsilon}(A-2,B)+\tilde{\epsilon}(A-1,2B+\tilde{\epsilon}[A-2,B]),\\
&E_4=4B+\tilde{\epsilon}(A-3,B)+\tilde{\epsilon}(A-2,2B+\tilde{\epsilon}[A-3,B])\\
&\qquad+\tilde{\epsilon}(A-1,3B+\tilde{\epsilon}[A-3,B]\\
&\qquad\quad+\tilde{\epsilon}[A-2,2B+\tilde{\epsilon}\{A-3,B\}]).
\end{aligned} \tag{A9}$$

If the dependence of a on A is neglected (this approximation seems reasonable for heavy target nuclei and where the mass range occupied by the spallation yield distribution is not too wide) so that $\tilde{\epsilon}$ no longer depends on A, then one can derive the following more convenient relationship:

$$E_{j+1}=E_j+B+\tilde{\epsilon}(E_j). \tag{A10}$$

Equation (A8) may be used, with the aid of Eq. (A9) or (A10) to calculate a spallation mass yield distribution below $A=\alpha$, if the function $P_\alpha(E)$ is available.[36,37]

Numerical calculations using Eqs. (A8) and (A10) reveal that if $d\log P_\alpha(E)/dE\leqslant 0$ and $d^2\log P_\alpha(E)/dE^2\leqslant 0$ for $E_j\leqslant E\leqslant E_{j+3}$ then $(\bar{\sigma}_{\alpha-j})(\bar{\sigma}_{\alpha-j-2})/(\bar{\sigma}_{\alpha-j-1})^2<1$, i.e., then $d^2\log\bar{\sigma}_A/dA^2<0$ for that portion of the smoothed $\log\bar{\sigma}_A$ curve for which $\alpha-j-2\leqslant A\leqslant\alpha-j$. In addition, numerical calculations show that for the smoothed curve of $P_A(E)$ for $A=192$, shown in Fig. 13, $d^2\log\bar{\sigma}_A/dA^2<0$ for all attainable $A<192$. These calculations demonstrate (although they certainly do not "prove")

[36] A mass yield curve for the spallation of copper by 1.8-Gev protons was calculated by the authors of reference 4 using the results of their Monte Carlo cascade calculations together with a few simple assumptions concerning the evaporation phase of the reaction. The application of these assumptions turns out to be almost equivalent to the use of Eq. (A8) to compute the mass yield curve, where instead of using Eqs. (A9) or (A10) the integrations are performed with the aid of the expression $E_{j+1}=E_j+B+2\tau$, where τ is a constant independent of E. This simple calculational procedure has also been employed by M. Lindner and A. Turkevich, Phys. Rev. **119**, 1632 (1960). Using the same "constant nuclear temperature" approximation, one can derive the expression

$$P_{A-j}(E)=P_A(E+j(B+2\tau)),\quad j=1, 2, 3, \cdots \tag{A11}$$

which is easier to use than Eq. (A5) and which should not be too inaccurate for j not too large.

[37] That the cross sections for the last few products at the low-mass end of the spallation distribution are underestimated by the above-described calculation, does not destroy the final conclusion, because (i) these cross sections are very small; and (ii) there are only a few of them.

the assertion made at the beginning of this Appendix. It is assumed that the qualitative observations which are made for 1.8-Gev incident protons are also valid for 5.7-Gev protons. That they may also be valid for about 0.5-Gev protons is suggested by the data of Kurchatov *et al.*[38] for the interactions of silver with 0.48-Gev protons; here, the smoothed log σ_A curves shows an over-all negative second derivative with respect to A which persists even while the σ_A decrease three orders of magnitude with decreasing A.

[38] B. V. Kurchatov, V. N. Mekhedov, N. I. Borisova, M. Ya. Kuznetsova, L. N. Kurchatova, and L. V. Chistyakov, *Proceedings of the Conference of the Academy of Sciences of the U.S.S.R. on the Peaceful Uses of Atomic Energy, Moscow,* July, 1955 (Akademiia Nauk, S.S.S.R., Moscow, 1955) [translation by Consultants Bureau, New York: Atomic Energy Commission Report TR-2435, 1956, p. 111].

PHYSICAL REVIEW VOLUME 126, NUMBER 4 MAY 15, 1962

Polarization in π^--p Scattering between 500 and 940 Mev*

E. F. BEALL, B. CORK,† P. G. MURPHY,‡ AND W. A. WENZEL
Lawrence Radiation Laboratory, University of California, Berkeley, California

AND

C. M. P. JOHNSON
Clarendon Laboratory, Oxford University, Oxford, England

AND

L. J. KOESTER, JR.§
Physics Department, University of Illinois, Urbana, Illinois

(Received December 22, 1961)

A graphite-plate spark chamber has been used to analyze the polarization of protons recoiling from π^--p scattering. The observations were made at 90° (c.m. system) pion scattering angle for seven incident pion energies between 500 and 940 Mev, at 120° or 135° for five energies in this interval, and also at 75° for 500 Mev only. The results are compared with predictions of several models used to explain the maxima in the π^--p scattering cross section. Qualitative arguments show that the energy intervals between these maxima are not completely dominated by neighboring single-state resonances. Phase shifts found to be large in scattering also seem to be large in polarization.

I. INTRODUCTION

THE first maximum in the pion-nucleon scattering cross section occurs at about 200-Mev incident kinetic energy and is well understood in terms of a resonant state with even parity, $\frac{3}{2}$ units of total angular momentum J, and $\frac{3}{2}$ units of total isotopic spin T. Interpretations of the higher maxima are less certain.[1] The second peak, at 600 Mev, has been interpreted[2] as a resonance with $T=\frac{1}{2}$, $J=\frac{3}{2}$, and odd parity ($D_{\frac{3}{3}}$). The $T=\frac{1}{2}$ assignment is based on the relative behavior of the π^-p and π^+p total cross sections[3–5] and on the ratio of π^+/π^0 photoproduction.[6] The $J=\frac{3}{2}$ assignment is favored by photoproduction angular distributions.[7,8] The odd parity assignment[9] is largely supported by the observation of substantial polarization of the recoil protons in photoproduction[10,11] at energies intermediate between the first-two maxima. Quantitative analyses of the differential cross sections for π^-p scattering give evidence for a large D-wave contribution but do not establish a resonance.[12] The third maximum in the pion-nucleon cross sections at 900 Mev has been interpreted[1,2] as a $T=\frac{1}{2}$, $F_{\frac{5}{3}}$ resonance. However, on the basis of the observed structure in the π^+p total cross section near 900 Mev,[4,5] the π^-p scattering is probably affected by the $T=\frac{3}{2}$ as well as $T=\frac{1}{2}$ states at these energies.

Moravcsik[13] has described a qualitative scheme for using the polarization of recoil protons from π^-p elastic

* Work performed under the auspices of the U. S. Atomic Energy Commission.

† Now on leave of absence at the European Organization for Nuclear Research (CERN), Geneva, Switzerland.

‡ Work done while on leave from the Rutherford High Energy Laboratory, Harwell, Didcot, Berks, England.

§ Supported in part by the U. S. Office of Naval Research.

[1] For a survey of elastic scattering data between 500 and 1000 Mev, see B. J. Moyer, Revs. Modern Phys. **33**, 367 (1961).

[2] R. F. Peierls, Phys. Rev. **118**, 325 (1960).

[3] H. C. Burrowes, D. O. Caldwell, D. H. Frisch, D. A. Hill, D. M. Ritson, R. A. Schluter, and M. A. Wahlig, Phys. Rev. Letters **2**, 119 (1959).

[4] J. C. Brisson, J. Detoef, P. Falk-Vairant, L. van Rossum, G. Valladas, and L. C. L. Yuan, Phys. Rev. Letters **3**, 561 (1959); Nuovo cimento **19**, 210 (1961).

[5] T. J. Devlin, B. C. Barish, W. N. Hess, V. Perez-Mendez, and J. Solomon, Phys. Rev. Letters **4**, 242 (1960).

[6] R. R. Wilson, Phys. Rev. **110**, 1212 (1958).

[7] F. P. Dixon and R. L. Walker, Phys. Rev. Letters **1**, 142, 458 (1958).

[8] J. I. Vette, Phys. Rev. **111**, 622 (1958).

[9] J. J. Sakurai, Phys. Rev. Letters **1**, 258 (1958).

[10] P. C. Stein, Phys. Rev. Letters **2**, 473 (1959).

[11] R. Querzoli, G. Salvini, and A. Silverman, Nuovo cimento **19**, 53 (1961).

[12] C. D. Wood, T. J. Devlin, J. A. Helland, M. J. Longo, B. J. Moyer, and V. Perez-Mendez, Phys. Rev. Letters **6**, 481 (1961).

[13] M. J. Moravcsik, Phys. Rev. **118**, 1615 (1960).